Contents lists available at ScienceDirect

Journal of Molecular Spectroscopy

journal homepage: www.elsevier.com

BerlinTrap: A new cryogenic 22-pole ion trap spectrometer

Alan Günther [a], Pablo Nieto [a], David Müller [a], Alexander Sheldrick [a], Dieter Gerlich [b], Otto Dopfer [a, *]

[a] Institut für Optik und Atomare Physik, Technische Universität Berlin, D-10623 Berlin, Germany
[b] Institut für Physik, Technische Universität Chemnitz, D-09107 Chemnitz, Germany

ARTICLE INFO

Article history:
Received 14 July 2016
Received in revised form 23 August 2016
Accepted 26 August 2016
Available online xxx

Keywords:
Cryogenic ion trap
He tagging
Solvation shell
Flavins
Spectroscopy
Photodissociation

ABSTRACT

The design and first applications of a new tandem mass spectrometer (BerlinTrap) combining an electrospray ion source, a quadrupole mass spectrometer, a cryogenic 22-pole ion trap (4–300 K), and an orthogonal reflectron time-of-flight mass spectrometer are described. The trapped ions are cooled by helium buffer gas cooling. The formation and solvation shell structure of weakly-bound $He_nH_3O^+$ complexes and the electronic photodissociation spectrum of the protonated amino acid tyrosine are used to calibrate the setup for cooling, tagging, and spectroscopic capabilities. A vibrational temperature below 20 K is inferred for protonated tyrosine. The electronic spectrum of isolated protonated lumichrome, the smallest protonated flavin, is recorded in the visible range and assigned to the most stable N5 isomer by comparison with quantum chemical calculations. These results demonstrate the suitability of the BerlinTrap apparatus for spectroscopy and reactivity studies of small and large (bio-)molecular ions and their clusters.

1. Introduction

The spectroscopic study of molecular ions has been a central topic for a broad span of scientific fields ranging from low-temperature physics, astrochemistry, and physical chemistry to biochemistry. Specifically, spectrosopic investigations of molecular ions of biological importance are particularly interesting as a crucial tool for the understanding of fundamental (bio-)chemical interactions [1–12]. Spectroscopic studies at low temperatures are often necessary to extract detailed information about the geometric and electronic structure of such complex ions and their clusters [12]. For this purpose, buffer gas cooling of ions in a cryogenic ion trap has become a popular method of choice [4–7,13–22], which appears to be a more generally applicable approach than the more traditional supersonic expansion techniques [3,8,23–37] and the recently developed technique of ion trapping in superfluid helium droplets [38–41]. In buffer gas cooling, a collision gas (mostly He or H_2) serves as thermally conducting medium between the cold walls of the trap and the trapped ions. The result is a reduction in temperature not only of the internal degrees of freedom but also of the kinetic energy of the trapped ions. This approach can be used to accumulate a large number of cold ions in the trap up to the space-charge limit (10^6 ions/cm^3) [42].

In practice, three different types of buffer-gas cooled cryogenic traps are mostly used, namely (i) linear multipoles, (ii) ring electrode traps, and (iii) 3D Paul traps [42]. Before loading into the trap and after extraction from the trap, ions usually have to be selected by a mass spectrometer. Therefore, linear multipole traps (with 4, 6, 8 or 22 electrodes) are often combined with one or more mass spectrometers [5–7,12,14,16,19–21,43–50]. However, it is not possible to detect in a mass-selective mode more than one reaction product in a single experimental cycle with such a spectrometer, when using popular quadrupole mass filters for ion analysis. This can be a disadvantage for measuring photodissociation spectra of larger biomolecules or clusters, which dissociate into many different fragments. Some groups solve this problem by coupling a ring electrode trap [51–53], a 3D Paul trap [4,5,13,45,54], or a planar multipole trap [55,56] to a time-of-flight mass spectrometer (TOF). In such instruments, typical ion temperatures in the 10–50 K range have been demonstrated. The combination of a cryogenic hexapole ion trap (26 K) and a Fourier-transform ion cyclotron resonance mass spectrometer (held at 10 K) has also been utilized for cluster ion spectroscopy [57]. In the case of linear multipole traps, ion temperatures of 10 K in a 22-pole [49], 9–15 K for a quadrupole trap [58–60], and 4 K in a wire quadrupole [46] have been reported. Depending on the molecular or cluster ion of interest, an appropriate ion source should be chosen. One of the most popular and versatile types is based on electrospray ionization (ESI). Being a smooth ionization technique, ESI allows for the generation of charged particles with nearly unlimited mass range (up to the size of single viruses [61]) without fragmentation.

To the best of our knowledge, the combination of a linear 22-pole trap with a reflectron time-of-flight (ReTOF) mass spectrometer in an orthogonal configuration has not been reported. Combining the capacity of the 22-pole trap for reaching low ion temperatures with single-cycle detection of all reaction products in a mass-selective mode, efficient high-resolution laser spectroscopy is possible for a wide range of molecular ions. In the present article, we describe the design and first applications of a new tandem mass spectrometer (Berlin-

* Corresponding author.
Email address: dopfer@physik.tu-berlin.de (O. Dopfer)

http://dx.doi.org/10.1016/j.jms.2016.08.017
0022-2852/

Trap) combining an ESI source, a quadrupole mass spectrometer, a cryogenically cooled 22-pole ion trap (4–300 K), and an orthogonal reflectron time-of-flight (ReTOF) mass spectrometer. Trapped ions are cooled by means of He buffer gas cooling. In first tagging experiments, the formation of cold $He_nH_3O^+$ clusters from bare H_3O^+ illustrates the low ion temperatures achieved in the 22-pole trap. The well-known UV photodissociation (UVPD) spectrum of the protonated amino acid tyrosine is then used to assess the performance of the BerlinTrap for spectroscopic studies of larger biomolecules and the achieved vibrational temperature of the ions. As a first new spectroscopic study in this setup, we present the visible electronic photodissociation (VISPD) spectrum of protonated lumichrome, the parent molecule of the large family of flavins, and determine its structure with the help of quantum chemical calculations.

2. BerlinTrap: A 4K-ESI-QPMS-22-Pole-ReTOF ion trap spectrometer

A sketch of the BerlinTrap apparatus is shown in Fig. 1. The 4K-ESI-QPMS-22-Pole-ReTOF ion trap tandem mass spectrometer has been designed for the realization of laser spectroscopic studies of cold (bio-)molecular ions. The ions under study are generated in an ESI source and are accumulated and thermalized in a short mini-quadrupole (miniQP). The ion bunch is then transferred via a hexapole (HP) ion guide or collision cell to an adjacent quadrupole mass spectrometer (QPMS) employed for mass selection of the parent ion under study. Using an electrostatic quadrupole bender (B), these ions are then either directed to a channeltron ion counter (CT) or to a cryogenic 22-pole ion trap via an octupole ion guide (OP). In the 22-pole trap mounted on a cryostat (Cryo), the ions are accumulated and cooled by a pulse of He buffer gas. They may also react with He or other atoms and molecules seeded in the He buffer gas. Subsequently, the cold ions are extracted into an orthogonal ReTOF mass spectrometer. In laser experiments, the cold ions are excited with pulsed laser radiation either (i) in the 22-pole trap, or (ii) on their way between the 22-pole and the ReTOF, or (iii) in the extraction region of the ReTOF, leading to resonant photofragmentation. All photodissociation spectra shown here are recorded for ions several microseconds before they enter the ReTOF (mode ii). The resulting photoproducts are then mass analyzed by the ReTOF. All salient parts of the BerlinTrap apparatus are described in detail in the following sections.

2.1. ESI source with mini-quadrupole

The apparatus is currently equipped with a modified ESI source taken from a commercial mass spectrometer (Varian, 1200MS). This includes the housing for the spray, the needle with electric feedthroughs, the transfer capillary, the skimmer, and the miniQP. The latter is used to accumulate and thermalize ions generated in the ESI source before further transfer toward the 22-pole trap. This miniQP consists of four rods (l = 58 mm) with diameters of d = 3.2 mm and an inner inscribed radius of r_0 = 1.6 mm. The radiofrequency (RF) signal of 8.9 MHz for driving the miniQP is provided by a signal generator (Rigol, DG1022), which is amplified (QRP-PA-2008, 10 W power amplifier) and transformed with a homemade transformer to a maximum voltage of 250 V. The trapping potential along the ion flight axis is generated by setting a voltage to the skimmer on one end and the miniQP exit lens on the other end. Both applied voltages are in the 10–20 V range while the miniQP bias is about 5 V. In order to extract a short ion pulse (~0.5 ms) from the miniQP into the adjacent hexapole, the exit lens is switched to a negative pulling voltage (typically a few tens of volts). For ESI generation of the ions, the needle voltage is typically kept in the 3.5–5 kV range and the counter electrode is set to 0.7–1.1 kV. Nitrogen is used as drying and nebulizing gas.

2.2. Hexapole and octupole ion guides

Two pumping stages with homebuilt ion guides transfer the ions under high vacuum conditions to the 22-pole trap. The first stage houses a hexapole (HP, l = 238 mm, d = 5 mm, r_0 = 5 mm) to transfer the ions from the miniQP chamber into the QPMS. The RF signal (6 MHz) is delivered by a signal generator (CGC instruments, RFG-50) adapted to the electric capacitance of the hexapole. Electrostatic entrance and exit lenses of the hexapole optimize the ion transport. The hexapole ion guide is equipped with a buffer gas cell mounted around half the rod length for optional collision-induced dissociation, tagging, or chemical reaction experiments. For this purpose, buffer gas pulses seeded with tagging or reaction gas are injected by a pulsed valve (Parker, General Valve). Furthermore, the hexapole may be used for photochemical reactions to generate new species (product ions), since it is optically accessible along the hexapole trap axis.

In the vacuum chamber connecting the 22-pole chamber with the QPMS chamber, the ions are guided by an octupole (OP, l = 231 mm,

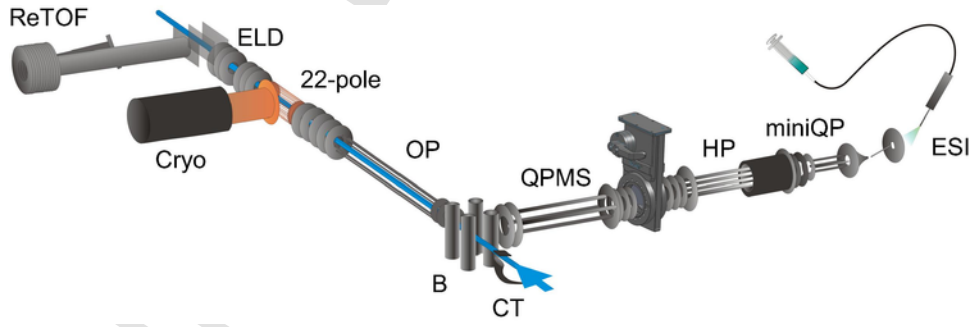

Fig. 1. Schematic diagram of the BerlinTrap apparatus (4K-ESI-QPMS-22-Pole-ReTOF ion trap tandem mass spectrometer). Ions generated in an electrospray ionization (ESI) source are accumulated and thermalized in a mini-quadrupole (miniQP). Subsequently, the ion bunch is transferred via a hexapole (HP) ion guide to a quadrupole mass spectrometer (QPMS) for size selection. With an electrostatic quadrupole bender (B), the mass-selected ions are either directed to a channeltron ion counter (CT) or toward a cryogenic 22-pole trap mounted on a cryostat (Cryo) via an octupole ion guide (OP). In the 22-pole trap, ions are cooled via buffer gas cooling using an intense He gas pulse. After tagging and/or interrogation with a laser pulse along the 22-pole axis (blue line), the ionic products are extracted and focused with the einzel lens deflector (ELD) into the acceleration region of the reflectron time-of-flight mass spectrometer (ReTOF), where they are detected with a microchannel plate detector.

d = 5 mm, r_0 = 7.5 mm). The same type of customized driver as used for the hexapole generates the RF signal with a maximum amplitude of 316 V at the resonance frequency of 3.6 MHz. An einzel lens stack mounted to the electrostatic quadrupole bender (B) focuses the ion beam into the octupole. A second stack with a split middle lens on the exit side of the octupole allows for optimized ion transfer into the 22-pole.

2.3. Quadrupole mass spectrometer with channeltron detector

A commercial quadrupole mass spectrometer (QPMS, Extrel, 150 QC) located after the hexapole is implemented to select the ions of interest from the products generated in the ESI source and/or the hexapole. A quadrupole ion bender (B) positioned after the QPMS can deflect the ions by 90° either to a channeltron detector (CT) or toward the 22-pole trap via the octupole. This configuration enables us to take a mass spectrum of the ions generated in the ESI source and/or the hexapole and thus simplifies the optimization of the beam intensity of the desired ion.

The QPMS including the bender and the channeltron is mounted on a CF DN150 flange. On this flange, an on-axis CF DN16 reduction flange is implemented and used for mounting a window to access the trapped ions by a laser beam. The QPMS has a triple-quad configuration (l = 211 mm, d = 19 mm, r_0 = 8.4 mm) in a housing made from stainless steel. It is driven by an 880 kHz RF signal generator and can filter masses in the *m*/*z* 1–1000 range. The transmitted mass is selected by means of a 0–10 V analog output of a DA/AD converter (National Instruments, PCI 6221) with 16 bit resolution, which also controls the applied bias voltage. Equipped with a conversion dynode, the efficiency of the channeltron to detect positive ions is enhanced. The detection of anions is also possible by changing the voltage polarity at the anode with respect to the channeltron. A pulse preamplifier (Advanced Research Instruments Cooperation, MTS-100) decouples the biased anode from the rest of the electronic data acquisition system.

2.4. Cryogenic 22-pole ion trap

The cryogenic 22-pole trap constitutes the heart of the BerlinTrap apparatus. The ion trap itself is built on two opposing copper plates. Each plate contains eleven commercially available syringe needles made from stainless steel that constitute the 22-pole trap (l = 36 mm, d = 1 mm, r_0 = 10 mm). Adjacent syringe needles belong to different plates. The two plates are mounted onto a copper base plate, electrically insulated and thermally connected by intervening sapphire plates. A copper lid covers the trap and eventually forms a closed buffer gas cell. The entrance and exit of the cell are formed by two electrostatic lenses with apertures of 5 mm diameter, which are separated from the rest of the trap by sapphire plates and spheres. The base plate of the 22-pole is mounted onto a brass block (Janis Research Co.) including two 50 Ω cartridge heaters and a Si diode temperature sensor (LakeShore, DT-670B-SD). The whole block is mounted onto the top of the coldhead of a two-stage closed-cycle helium cryostat (Cryo, Sumitomo, SRDK-408D2-F50H). A second Si diode is positioned on top of the 22-pole to measure its temperature. The two temperatures are monitored and regulated by a PID controller (LakeShore, 336). To reduce heating by thermal radiation, a second cold shield connected to the first stage of the coldhead (~40 W at 40 K) covers the 22-pole cell. Two einzel lenses fixed to the entrance and exit of the trap allow for optimizing the ion transport. The cooling power of the second stage of the coldhead is 1 W at 4.2 K, and thus thermal loads have to be reduced to a minimum. Stainless steel wires are employed for electric contact of the lenses. Thermal anchoring is made via ceramics fixed to the outer cold shield. The electric connection of the 22-pole is accomplished by thermally anchored titanium wires with 0.25 mm diameter. Titanium is preferred over iron due to its similar thermal conductivity but lower electrical resistivity. The RF power to drive the 22-pole trap is generated by the same type of power supply as used for the miniQP. It delivers a 7 MHz RF signal with maximum amplitude of 350 V.

To cool the trapped ions, a buffer gas is required as thermally conductive medium between the cold walls and the trapped ions. A fast piezo valve designed by Gerlich [62] is connected to the trap via a short Teflon tube and provides long intense gas pulses (typically 1–5 ms, 0.9 bar backing pressure) of He (Air Liquide, Helium N50). The ions enter the 22-pole when the He buffer gas pressure is highest, which maximizes the number of ions accumulated in the cryogenic trap. Different mixtures of buffer gases may be used to form different types of clusters in the trap via three-body collisions and/or chemical reaction. The typical trapping time of the ions in the 22-pole is around 100 ms, while trapping times as long as 15 min without any measurable ion loss are observed for Cs^+ (Fig. S1 in SI).

2.5. Ion deflector and ReTOF

After the ions are trapped and cooled in the 22-pole, push and pull voltage pulses are applied to the end caps of the trap to extract the ions as a short bunch into the acceleration region of the ReTOF. On their way, the ions pass the einzel lens deflector (ELD), which is an einzel lens stack with the middle lens split into four sections. This lens deflector enables focusing and deflecting ions into the acceleration region of the ReTOF. The shape and length of the ion bunch can be manipulated by the extraction voltages of the 22-pole end caps, and the voltages applied to the 22-pole exit lenses and the ELD. The ReTOF comprises a homebuilt Wiley-McLaren TOF with a total length of about 100 cm and a two-stage reflector made out of a stack of 13 ring electrodes, yielding a mass resolution of $m/\Delta m > 240$ under typical operation conditions. The ion detector employs two 50 mm diameter microchannel plates (MCP) mounted in chevron configuration (Tectra, MCP 50DLA). High voltage pulses applied to the acceleration electrodes of the ReTOF are supplied by two push–pull fast switches (Behlke, GHTS 60).

The ion extraction out of the 22-pole trap already acts as a simple low-resolution TOF spectrometer and partial mass separation occurs between the extraction from the 22-pole and the arrival at the ReTOF. As the diameter of the ReTOF acceleration region is limited (37 mm), only ions that are between the ReTOF plates (d = 15 mm) at the trigger time of the high voltage extraction pulses reach the MCP detector. This effect causes the relative intensities for different mass peaks to substantially depend on the delay between the 22-pole and ReTOF extraction pulses. To compensate for this delay dependence, mass spectra for different delays are measured and added up to obtain a mass spectrum of different ions in the 22-pole trap with reliable intensities (as is demonstrated in the $He_nH_3O^+$ cluster formation experiments described in Section 3.1). Photofragmentation of ions performed in the extraction region of the ReTOF is not affected by this effect.

2.6. Vacuum system

Ultra-high vacuum (UHV) conditions are required for proper cooling without effective adsorption of background gas in the 22-pole trap. To realize such UHV conditions in the 22-pole chamber, while having simultaneously low vacuum conditions in the ESI source

chamber, all chambers are separated by small apertures and evacuated separately by differential pumping. The miniQP chamber is evacuated using a 230 l/s turbomolecular pump (Pfeiffer, TMU 261 P). The other chambers (HP, B and QPMS, OP, ReTOF) are pumped by 240 l/s turbomolecular pumps (Pfeiffer, TPU 240), whereas the 22-pole stage is evacuated by a 700 l/s turbomolecular pump (Pfeiffer, Hi-Pace 700). The overall setup is also separated into two parts by a vacuum gate valve (VAT) installed between the hexapole and the QPMS chambers. It is implemented to enable maintenance of the ESI source without venting the rest of the apparatus. For all turbomolecular pumps at the 22-pole side of this valve, a 35 m^3/h scroll pump (Edwards, xds35i) serves as backing pump. To account for the high gas load at the miniQP and hexapole stages, a roots blower (Leybold, RUVAC WA251) combined with a 65 m^3/h rotary vane pump (Leybold, TRIVAC D65B) are used to achieve low backing pressure. The ESI source is separately pumped by a 20 m^3/h backing pump (Pfeiffer, Duo 20M). The pressures are measured by compact full range gauges (Balzers, PKR 251) in the low vacuum stages and by cold cathode gauges (Balzers, IKR260/270) for the high vacuum stages. The pressures are read out via a controller (Balzers, TPG 256 A). Typical pressures are in the 10^{-3}, 10^{-5}, and 10^{-7} mbar ranges for the miniQP, hexapole, and QPMS chambers with and without ESI operation, respectively. The pressures with ESI and He buffer gas pulses on/off are typically $1 \cdot 10^{-6}/2 \cdot 10^{-8}$ mbar for the octupole, $7 \cdot 10^{-6}/3 \cdot 10^{-8}$ mbar for the 22-pole, and $1 \cdot 10^{-6}/5 \cdot 10^{-9}$ mbar for the ReTOF chamber.

2.7. Laser system

The BerlinTrap apparatus has been designed to enable vibrational and electronic laser spectroscopy of cold trapped molecular (cluster) ions using pulsed and tunable IR and UV–vis lasers. The low ion density achieved in the trap requires high-power lasers. Pulsed optical parametric oscillator (OPO) lasers pumped by Q-switched nanosecond Nd:YAG lasers provide high output power and broad spectral tuning range. The experiments discussed below utilize a midband UV–vis OPO laser (Continuum, Panther EX-OPO) pumped by the third harmonic of a Nd:YAG laser (Continuum, Powerlite DLS 9010). It provides laser pulses in the 205–2550 nm range with energies up to 70 mJ per pulse at 450 nm, 3–7 ns pulse length, and a bandwidth of about 2 cm^{-1} at a repetition rate of 10 Hz. The flash lamps and Q-switch are triggered externally. The laser radiation is calibrated to an accuracy of ± 2 cm^{-1} using a wavelength meter (Bristol Instruments, 821). The OPO laser beam enters the 22-pole from the channeltron side and exits the spectrometer through a window after the ReTOF extraction region. The laser intensity is monitored after passing through the apparatus with a power meter (OPHIR, Vega). Spectroscopic information in form of VIS or UV photodissociation (VISPD or UVPD) is obtained by resonant absorption of one or more photons and subsequent fragmentation of the molecular (cluster) ions.

2.8. Voltage supplies and data acquisition system

The BerlinTrap setup contains more than 50 components requiring separate DC power supplies. 40 of them are controlled by two amplifiers (Spectrum Solutions Inc., TDI 400), each providing 20 independent voltage outputs with up to ± 400 V. These voltages are set by three analog output boards (ICPDAS, PIO-DA16) with 16 channels each and 14 bit resolution, which are computer controlled via LabView programs. Some electrostatic lenses, e.g., the miniQP or 22-pole end caps, must be operated in a pulsed mode. These voltage pulses are delivered by five signal generators (Rigol, DG1022) with periods from 2000 s down to 500 ns and rise times of 20 ns for 10 Hz pulses with maximum amplitude of 20 V. The length and delay of the pulses can only be controlled for positive edges. One-to-one voltage inverter circuits between the pulse generators and the lenses solve this problem. To amplify to higher voltages up to ± 175 V, voltage amplifiers (Falco Systems, WMA02) with rise times of up to 40 μs are employed. Synchronization of the laser pulse with the ion trap experiment is achieved by a digital pulse and delay generator (Berkeley Nucleonics Corporation, 575) with maximum time resolution of 250 ps. Two channels are used to separately trigger the flash lamps and the Q-switch of the Nd:YAG pump laser of the OPO laser. The delay generator acts also as the master clock of the whole experiment and triggers all other pulsed voltages. Preamplified signals from the channeltron are registered with a DA/AD converter (National Instruments, PCI 6221). The ion signal detected at the MCP detector in the ReTOF after preamplification (ORTEC, 9305 fast preamplifier) is time resolved at the nanosecond time regime, monitored, and registered with a digitizer card (Agilent, U1070A-001).

3. Applications

3.1. Tagging of H_3O^+ with He atoms

The ion storage and cooling performance of the BerlinTrap is explored by monitoring its tagging efficiency for hydronium ions. Distilled water is sprayed at a rate of 0.5 ml/h to generate H_3O^+ ions in the ESI source. The H_3O^+ ion bunches accumulated in the miniQP are transferred into the 22-pole. A He pulse of about 4.5 ms is injected into the 22-pole trap at about 1.5 ms before the ions leave the miniQP, so that they enter the trap at maximum He pressure. This experimental time sequence is needed to enhance both the trapping efficiency and the probability for tagging via three-body collisions of the type

$$He_{n-1}H_3O^+ + 2\ He \rightarrow He_nH_3O^+ + He$$

in the 22-pole trap. After a trapping time of 95 ms in the 22-pole held at 5 K, the ions are extracted from the trap and analyzed in the ReTOF. Due to their different mass, each $He_nH_3O^+$ complex enters the ReTOF extraction region at a different time, thereby affecting the relative intensities of its mass peak as explained in Section 2.5. To compensate for this delay dependence, a scan of the delay time between the 22-pole and ReTOF extraction pulses is accomplished by taking mass spectra for different delays (every 2 μs) and adding them up. The result of the averaged spectrum is shown in Fig. 2, while selected individual mass spectra are available in Fig. S2 in SI. Complexes with up to five He atoms attached to H_3O^+ are observed. The main features of the mass spectrum shown in Fig. 2 as semi-logarithmic plot are a small relative increase of the n = 3 cluster and a sharp intensity drop for the n = 4 and 5 clusters. These results are comparable with those obtained by Asvany et al. [43] in a similar 22-pole setup and hence the low ion temperature should be of the same order, too.

The sharp drop in intensity at n = 4 can readily be rationalized by considering that three He atoms can bind relatively strongly to the three available equivalent protons of H_3O^+, while the fourth and the fifth He atom fill a second solvation shell with significantly lower binding energy. Global minima for the different $He_nH_3O^+$ clusters are determined by quantum chemical calculations at the CCSD/aug-cc-pVTZ level, with subsequent single-point energy calculations at the CCSD(T)/aug-cc-pVTZ level [63]. Equilibrium structures and total binding energies for the complexes are available in Fig. S3 and

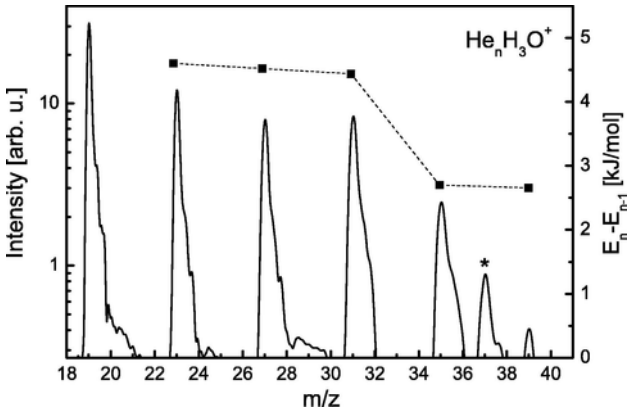

Fig. 2. He-tagging of H_3O^+ in the 22-pole trap. Mass spectrum of $He_nH_3O^+$ complexes (on a logarithmic y1-axis) grown in the 22-pole trap from H_3O^+ ions generated in the ESI source by interaction with a pulse of intense He buffer gas. The mass spectrum is averaged over various delays between the 22-pole and ReTOF extraction pulses. The peak marked with an asterisk corresponds to the $H_5O_2^+$ cluster (*m*/*z* 37) formed from water contamination in the trap. The filled squares connected by the dashed line and the linear y2-axis scale give the gain in total binding energy of the $He_nH_3O^+$ complexes for each added He atom (CCSD(T)/aug-cc-pVTZ).

Table S1 of SI. The incremental binding energy for the addition of an extra He atom ($E_n - E_{n-1}$) of 4.60, 4.53, 4.44, 2.70, 2.65, and 2.55 kJ/mol for n = 1–6 is also plotted in Fig. 2 on a linear scale. The first three He ligands bind indeed nearly linearly to the three protons via O—H···He hydrogen bonding and are symmetrically located around the C_3 symmetry axis of H_3O^+. The incremental binding energy in the first shell (n = 1–3) is roughly twice the one in the second shell (n = 4–6), which also can accommodate three He atoms. In the n = 6 complex, the six He ligands form a nearly planar six-membered ring around the C_3 symmetry axis. The high and comparable abundance of the n = 1–3 clusters thus indicates similarly strong bonding in the first solvation shell, while the large drop toward larger n is given by the lower binding energies in the second shell and the strongly decreasing probability for formation of larger clusters due to the limited number of collisions within the finite He pulse length.

3.2. UVPD spectrum and vibrational temperature of protonated tyrosine

Although the $He_nH_3O^+$ cluster formation experiments described in Section 3.1 yield qualitative information on the cooling performance of the BerlinTrap, the temperature for the internal degrees of freedom of the trapped ions shall be determined in a more accurate way. To this end, we characterize the effective vibrational temperature of trapped biomolecules in the cryogenic ion trap by evaluating the intensities of hot bands of the protonated amino acid tyrosine (H^+Tyr) involving low-frequency modes in the spectrum of its electronic S_1-S_0 transition measured by UVPD spectroscopy. H^+Tyr has been used in the past by other groups as a benchmark to evaluate the effective vibrational temperature of biomolecular ions stored in cryogenic traps [44,49,64]. The H^+Tyr ions are generated by spraying a mixture of 1.5 mg of tyrosine (Carl Roth, >99%) dissolved in a mixture of 13 ml methanol, 7 ml water, and 1 ml acetic acid at a rate of 4 ml/h. The main fragments observed upon UVPD of H^+Tyr for resonant excitation of its S_1-S_0 transition are the ions with *m*/*z* 108 and 136. Significantly, the action spectra recorded in both fragment channels are quite different (Fig. S4 in SI) because the fragmentation ratio depends strongly on the conformer, underlying the invaluable advantage of simultaneous TOF analysis of all dissociation products, as used here in the BerlinTrap setup. The UVPD spectrum monitored in the more intense fragment channel (*m*/*z* 108) [44,65,66] is shown in Fig. 3 for a nominal ion trap temperature of 5 K, while spectra for higher trap temperatures (5–70 K) are compared in Fig. 4. The UVPD spectrum obtained in the present work is in good agreement with the ones reported previously [44,49,64]. The S_1-S_0 band origins (0-0) for the four conformers of H^+Tyr, labeled A_{0-0}-D_{0-0}, are located at 35,081, 35,111, 35,185, and 35,235 cm^{-1}, respectively. Hot bands occurring at frequencies lower than the A_{0-0} band are also resolved in the UVPD spectra.

The thermal population of the vibrationally excited states of the various H^+Tyr conformers can be used to estimate the effective vibrational temperature of the trapped ions assuming thermodynamic equilibrium. The frequency of the lowest vibrational mode of the B conformer of H^+Tyr is determined as $\Delta E = 43$ cm^{-1} by measuring the difference between the hot band transition (B_{0-1}, 35,068 cm^{-1}) and the

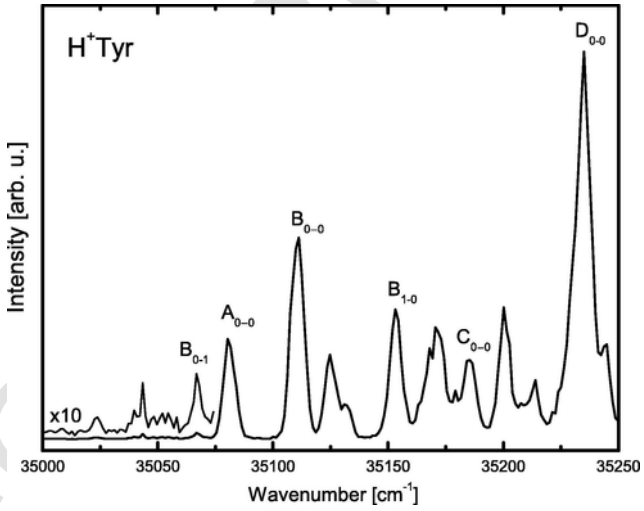

Fig. 3. UVPD spectrum of the protonated amino acid tyrosine. UVPD spectrum of the S_1-S_0 electronic transition of H^+Tyr for a 22-pole trap temperature of 4 K. The UVPD signal is obtained by monitoring the fragment *m*/*z* 108, linearly normalized for variations in the laser power and parent ion signal (*m*/*z* 182). The S_1 band origins (0-0) for the four different conformers (A-D) as well as the bands used for the estimation of the vibrational ion temperature are labeled.

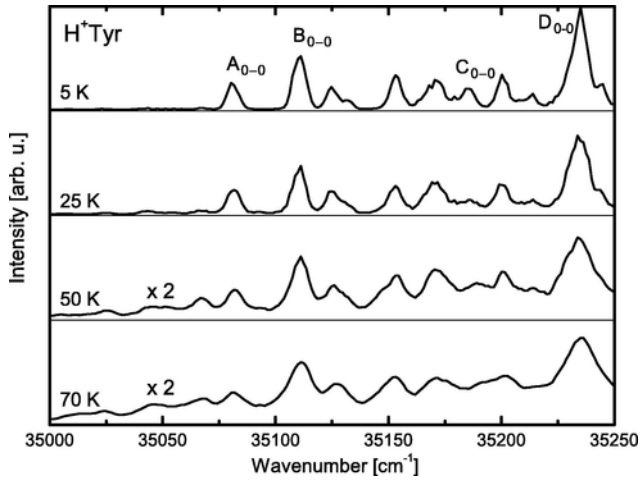

Fig. 4. UVPD spectra of protonated tyrosine (H^+Tyr) for different 22-pole trap temperatures. The S_1 band origins (0-0) for the four different conformers (A-D) are labeled. If not indicated otherwise, all spectra are drawn to the same scale.

band origin ($B_{0\text{-}0}$, 35,111 cm^{-1}). To calculate the temperature, the intensity ratio between these two transitions may be used. This requires the determination of the Franck-Condon factors for both transitions. To this end, CC2/aug-cc-pVDZ calculations are carried out for the B isomer for the ground (S_0) and first electronically excited (S_1) singlet states [67]. Franck-Condon simulations for different temperatures using PGOPHER [68] result in an effective vibrational temperature of 17.2 ± 2.3 K for the UVPD spectrum in Fig. 3.

Along a second route, the ion vibrational temperature may also be estimated without the knowledge of Franck-Condon factors. As the normal modes in the S_0 ground state are similar to the ones of the electronically excited S_1 state, the Franck-Condon factors of the $B_{0\text{-}1}$ and $B_{1\text{-}0}$ transitions are quite similar (here calculated as $1.2 \cdot 10^{-3}$ and $1.0 \cdot 10^{-3}$, respectively, using the FC-Lab II program [69]), and those transition intensities may then directly be used for the evaluation of the vibrational temperature. In that case, the intensity ratio is merely given by the population ratio between the ground (v = 0) and excited vibrational state (v = 1) and, hence, the vibrational ion temperature can be estimated from the intensity ratio between these two transitions ($B_{0\text{-}1}$, $B_{1\text{-}0}$). Using this method, the effective temperature is given by

$$T = -\frac{\Delta E}{k_B \cdot \ln\left(\frac{I_{B_{0-1}}}{I_{B_{1-0}}}\right)}$$

and the vibrational temperature for the B conformer of H^+Tyr is estimated as 17.9 ± 2.0 K at a nominal trap temperature measured as 5 ± 1 K, in excellent agreement with the temperature of 17.2 ± 2.3 K derived directly from the Franck-Condon simulations. The UVPD spectra measured at higher trap temperatures in Fig. 4 exhibit band broadening and the appearance of a broad background due to the population of higher vibrational and rotational levels for all four H^+Tyr conformers, illustrating the need of low temperature for the spectroscopy of biomolecular ions.

3.3. VISPD spectrum and structure of protonated lumichrome

The BerlinTrap has initially been designed for the laser spectroscopic study of the structure and photochemical properties of isolated and microsolvated biomolecules, and specifically protonated and metalated flavins. This fundamental class of biomolecules is ubiquitous in biological systems and particularly important because of their photochemistry regulating, for instance, light-induced reactions of blue light photoreceptors [70–74]. In our previous studies, the structures of simple protonated and metalated flavins have been determined by means of IR multiphoton dissociation (IRMPD) in a room temperature ion trap combined with density functional theory calculations [29,75,76]. Specifically, the N5 atom has been identified as the preferred protonation site of the simplest protonated flavin, namely protonated lumichrome (H^+LC) [76]. Herein we explore the absorption spectrum of cryogenically cooled H^+LC ions in the optical range by VISPD spectroscopy of its electronic S_1-S_0 transition.

For the formation of protonated lumichrome (Sigma Aldrich, >99%), 2 mg of the neutral molecule are added to a solution of 17 ml methanol, 1 ml water, and 2.5 ml formic acid. The solution is sprayed at a rate of 2 ml/h. The mass spectra of cold H^+LC ions measured with the OPO laser on (solid line) and off (dotted line) at the strong S_1 origin resonance (19,962 cm^{-1}) are compared in Fig. 5. The intensity of the H^+LC parent ion (*m*/*z* 243) is about 150 times stronger than the intensity of the most abundant laser-induced fragments ob-

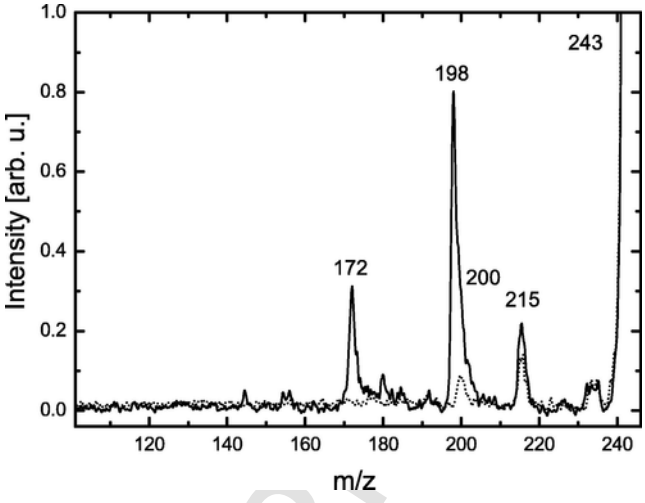

Fig. 5. Photodissociation mass spectra of protonated lumichrome. Laser-on (solid line) and laser-off (dotted line) mass spectra of H^+LC (*m*/*z* 243) with the laser frequency tuned resonantly to the electronic S_1 band origin at 19,962 cm^{-1} (see Fig. 6 for a full VISPD spectrum).

served at *m*/*z* 172 and 198 (a weak fragment at *m*/*z* 200 is not fully resolved). A further minor dissociation channel occurs at *m*/*z* 215. In the previous IRMPD experiments [76], the same main fragment ions are observed at *m*/*z* 172, 198, and 200. The similar fragment channels observed for IRMPD and VISPD suggest that optical excitation of the S_1 state is followed by internal conversion to the S_0 ground state and subsequent statistical dissociation.

The VISPD spectrum of H^+LC shown in Fig. 6 is obtained by monitoring the two predominant fragment ion signals (*m*/*z* 172 and 198), linearly normalized for laser power and parent ion intensity (*m*/*z* 243). The nominal 22-pole trap temperature is kept at 25 K to maximize the VISPD signal. The intense S_1 band origin is observed at 19,962 cm^{-1}, and many intense vibronic transitions are detected toward higher frequency, indicating a substantial geometry change upon electronic excitation. The measured bands have a width of the order of 6 cm^{-1}, which results from a combination of unresolved rotational structure and the limited laser bandwidth of 2 cm^{-1}. No noticeable hot bands are detected toward lower frequency of the S_1 origin. These observations are consistent with a rovibrational temperature of 25 K.

The H^+LC(N5) isomer with protonation at N5 has been identified as global minimum in previous B3LYP/cc-pVDZ calculations and has indeed been the only isomer observed in the experimental IRMPD spectra of room-temperature ions [76]. H^+LC isomers with protonation at other nucleophilic binding sites (O4, N10, O2) as well as protonation of iso-lumichrome have been predicted to be less stable by at least 20 kJ/mol [76]. Here, quantum chemical calculations [63] are carried out for the various low-energy H^+LC isomers using time-dependent density functional theory at the PBE0/cc-pVDZ level to predict their electronic spectra and to assign the measured VISPD spectrum. The calculated adiabatic S_1 origin transitions of the isomers shown in Fig. S5 in SI are listed in Table 1, along with their shift from the experimental value (19,962 cm^{-1}) and their relative proton affinities. The N5 isomer turns out to be the global minimum also at the PBE0/cc-pVDZ level, with an energy gap of more than 1600 cm^{-1} (19 kJ/mol) to higher-energy isomers. In addition, it is also the isomer with the S_1 origin predicted closest to the observed one ($\Delta S_1 = -809$ cm^{-1}). It is interesting to note that the S_1 origin shift induced by protonation is remarkably large (5673 cm^{-1} or 0.70 eV) from that predicted at 24,826 cm^{-1} for bare LC. This result emphasizes the drastic impact of protonation on the electronic structure of

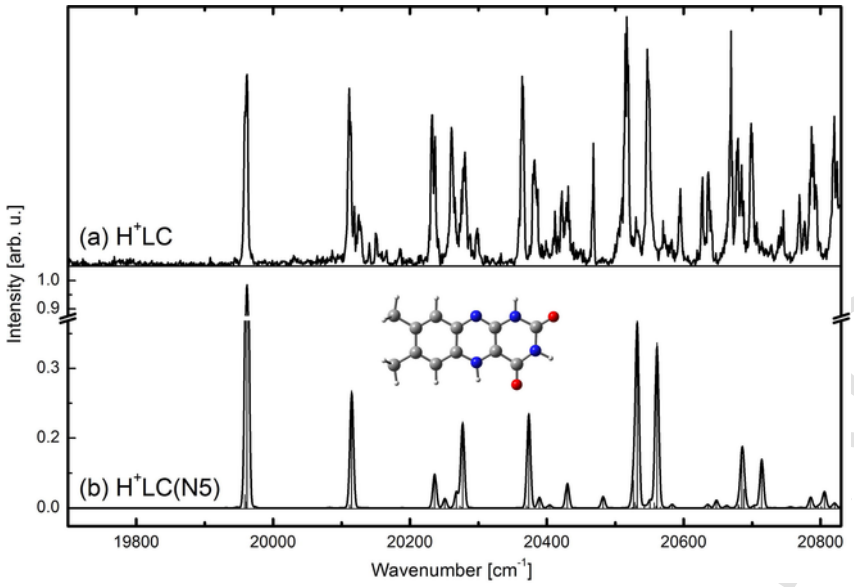

Fig. 6. Electronic photodissociation spectrum of protonated lumichrome. (a) Experimental VISPD spectrum of the S_1-S_0 transition of protonated lumichrome (H^+LC) recorded for a trap temperature of 25 K and (b) Franck-Condon simulation for the N5 isomer of H^+LC based on quantum chemical calculations at the PBE0/cc-pVDZ level for a vibrational ion temperature of 25 K. The simulated spectrum has been shifted by +809 cm^{-1} to match the experimental band origin.

Table 1
Calculated S_1 band origins of LC and various H^+LC isomers and their difference (ΔS_1) to the measured S_1 origin at 19,962 cm^{-1}. Relative proton affinities (ΔS_0) of the ground state are also given. All energies include harmonic zero-point vibrational energies. The absolute value for the proton affinity of H^+LC(N5) is calculated as 969 kJ/mol.

	S_1 [cm^{-1}]	ΔS_1 [cm^{-1}]	ΔS_0 [cm^{-1}]
LC	24,826		
H^+LC(N5)	19,153	−809	0
H^+LC(O4)	18,451	−1511	1612
H^+LC(N10)	22,555	2593	2630
H^+LC(O2)	22,422	2460	5828
H^+isoLC(N5)	15,437	−4525	6539

flavins. It is expected that the interaction of LC with alkali and other (transition) metal ions induces similarly large red shifts of variable magnitude depending on the size, type, charge, binding site, and binding energy of the ion, and investigations in that direction are currently underway using the BerlinTrap.

Franck-Condon simulations are employed to confirm the assignment of the measured H^+LC spectrum to the N5 isomer. The spectrum simulated for T = 25 K is compared in Fig. 6 to the measured one, using a convolution with Gaussian line profiles with 6 cm^{-1} FWHM. Although the intensity of the S_1 origin transition is somewhat overestimated (note the break in the vertical scale) the main vibronic features are well reproduced by the Franck-Condon simulations confirming the isomer assignment to H^+LC(N5). This conclusion is strengthened further by the Franck-Condon simulation for the next stable O4 isomer, which poorly reproduces the measured VISPD spectrum (Fig. S6 in SI). A detailed discussion of the electronic properties and the optical spectra of the various H^+LC isomers will be reported elsewhere.

4. Conclusions

We have described the design and first applications of the BerlinTrap, a new type of cryogenic 4K-ESI-QPMS-22-Pole-ReTOF ion trap tandem mass spectrometer suitable for the laser spectroscopic characterization of molecular (cluster) ions. It combines the advantages of (i) ion generation by ESI, (ii) cryogenic buffer gas cooling of mass-selected ions trapped in a 22-pole, and (iii) simultaneous mass-selective detection of all product ions issued from laser photodissociation or chemical reaction (including cluster growth) in a single experimental cycle using a ReTOF. The efficiency and performance of the setup have been demonstrated by the formation of weakly-bound $He_nH_3O^+$ clusters in the 22-pole trap, which exhibit the formation of distinct solvation shells. In addition, the analysis of the vibrationally-resolved UVPD spectrum of the protonated amino acid H^+Tyr confirms cooling of the vibrational temperature of biomolecular ions to below 20 K in the 22-pole trap.

As a final application, the electronic spectrum of protonated lumichrome (H^+LC) has been recorded and analyzed by VISPD spectroscopy and quantum chemical calculations. Significantly, the VISPD spectrum of H^+LC corresponds to the first optical spectrum of any flavin molecule isolated in the gas phase. The analysis of the S_1 band origin and vibronic spectrum via Franck-Condon simulations is consistent with the detection of the most stable N5 isomer of H^+LC, which has been identified previously by IRMPD spectroscopy of ions trapped at 300 K in an ICR cell. Interestingly, the large protonation-induced red shift of the S_1 origin detected at 19,962 cm^{-1} (ΔS_1 = 5673 cm^{-1}, 0.70 eV, 23%) confirms the substantial impact of protonation on the electronic structure of this prototypical flavin. Currently, similar optical studies are underway for the related metalated lumichrome (M^{q+}LC) complexes with alkali and other metal ions, which will elucidate the perturbation of the electronic structure as a function of the M^{q+} charge, type, binding site, and bond strength.

Acknowledgments

This work was supported by Deutsche Forschungsgemeinshaft (DFG, grant number DO 729/6). We thank TU Chemnitz and Deutsche Forschungsgemeinschaft for the generous continuous loan of the ESI source, the 22-pole trap, and several turbomolecular pumps. We thank Stephan Schlemmer and Christoph Konietzko for providing the piezo valve. Fruitful discussions with Oleg Boyarkine,

Oskar Asvany, Stephan Schlemmer, Sven Fanghänel, Corey Rice, Nadja Heine, and Ulrich Lorenz are gratefully acknowledged. Judith Langer, Markus Schütz, Tim Wandrey, and Thu Trang Trinh are thanked for technical support in the initial stage of the development of the apparatus.

Appendix A. Supplementary data

Supplementary data associated with this article can be found, in the online version, at http://dx.doi.org/10.1016/j.jms.2016.08.017.

References

[1] M.A. Rijs, J. Oomens (Eds.), Gas-Phase IR Spectroscopy and Structure of Biological Molecules, Springer International Publishing, Cham, 2015.
[2] J-P. Schermann, Spectroscopy and Modelling of Molecular Building Blocks, first ed., Elsevier, Amsterdam, Boston, 2008.
[3] J.R. Roscioli, L.R. McCunn, M.A. Johnson, Science 316 (2007) 249–254.
[4] E. Garand, M.Z. Kamrath, P.A. Jordan, A.B. Wolk, C.M. Leavitt, A.B. McCoy, S.J. Miller, M.A. Johnson, Science 335 (2012) 694–698.
[5] A.B. Wolk, C.M. Leavitt, E. Garand, M.A. Johnson, Acc. Chem. Res. 47 (2014) 202–210.
[6] J. Roithová, A. Gray, E. Andris, J. Jašík, D. Gerlich, Acc. Chem. Res. 49 (2016) 223–230.
[7] T.R. Rizzo, J.A. Stearns, O.V. Boyarkin, Int. Rev. Phys. Chem. 28 (2009) 481–515.
[8] A. Bouchet, M. Schütz, B. Chiavarino, M.E. Crestoni, S. Fornarini, O. Dopfer, Phys. Chem. Chem. Phys. 17 (2015) 25742–25754.
[9] O. Dopfer, M. Fujii, Chem. Rev. 116 (2016) 5432–5463.
[10] K. Sakota, M. Schütz, M. Schmies, R. Moritz, A. Bouchet, T. Ikeda, Y. Kouno, H. Sekiya, O. Dopfer, Phys. Chem. Chem. Phys. 16 (2014) 3798–3806.
[11] K. Tanabe, M. Miyazaki, M. Schmies, A. Patzer, M. Schütz, H. Sekiya, M. Sakai, O. Dopfer, M. Fujii, Angew. Chem. Int. Ed. 51 (2012) 6604–6607.
[12] T.R. Rizzo, O.V. Boyarkin, in: M.A. Rijs, J. Oomens (Eds.), Gas-Phase IR Spectroscopy and Structure of Biological Molecules, Springer International Publishing, Cham, 2015, pp. 43–97.
[13] G. Gregoire, C. Jouvet, C. Dedonder, A.L. Sobolewski, J. Am. Chem. Soc. 129 (2007) 6223–6231.
[14] N.S. Nagornova, T.R. Rizzo, O.V. Boyarkin, Science 336 (2012) 320–323.
[15] O. Asvany, P. Kumar, B. Redlich, I. Hegemann, S. Schlemmer, D. Marx, Science 309 (2005) 1219–1222.
[16] O. Asvany, K.M.T. Yamada, S. Brünken, A. Potapov, S. Schlemmer, Science 347 (2015) 1346–1349.
[17] M. Savoca, T. Wende, L. Jiang, J. Langer, G. Meijer, O. Dopfer, K.R. Asmis, J. Phys. Chem. Lett. 2 (2011) 2052–2056.
[18] K.R. Asmis, J. Sauer, Mass Spectrom. Rev. 26 (2007) 542–562.
[19] E.K. Campbell, M. Holz, D. Gerlich, J.P. Maier, Nature 523 (2015) 322–323.
[20] S. Chakrabarty, M. Holz, E.K. Campbell, A. Banerjee, D. Gerlich, J.P. Maier, J. Phys. Chem. Lett. 4 (2013) 4051–4054.
[21] C.A. Rice, F.-X. Hardy, O. Gause, J.P. Maier, J. Phys. Chem. Lett. 5 (2014) 942–945.
[22] A. Fujihara, H. Matsumoto, Y. Shibata, H. Ishikawa, K. Fuke, J. Phys. Chem. A 112 (2008) 1457–1463.
[23] E.J. Bieske, A.M. Soliva, A. Friedmann, J.P. Maier, J. Chem. Phys. 96 (1992) 28–34.
[24] E.J. Bieske, S. Nizkorodov, A. Friedmann, J.P. Maier, Int. J. Mass Spectrom. 135 (1994) 19–30.
[25] E.J. Bieske, O. Dopfer, Chem. Rev. 100 (2000) 3963–3998.
[26] P. Hobza, K. Müller-Dethlefs, Non-Covalent Interactions, RSC Publ, Cambridge, 2010.
[27] M.A. Duncan, J. Phys. Chem. A 116 (2012) 11477–11491.
[28] O. Dopfer, Z. Phys, Chem. 219 (2005) 125–168.
[29] A. Günther, P. Nieto, G. Berden, J. Oomens, O. Dopfer, Phys. Chem. Chem. Phys. 16 (2014) 14161–14171.
[30] A. Patzer, M. Schütz, C. Jouvet, O. Dopfer, J. Phys. Chem. A 117 (2013) 9785–9793.
[31] A. Patzer, M. Schütz, T. Möller, O. Dopfer, Angew. Chem. Int. Ed. 51 (2012) 4925–4929.
[32] M. Savoca, J. Langer, O. Dopfer, Angew. Chem. Int. Ed. 52 (2013) 1568–1571.
[33] M. Schmies, A. Patzer, M. Schütz, M. Miyazaki, M. Fujii, O. Dopfer, Phys. Chem. Chem. Phys. 16 (2014) 7980–7995.
[34] H.-S. Andrei, N. Solca, O. Dopfer, Angew. Chem. Int. Ed. 47 (2008) 395–397.
[35] A. Patzer, S. Chakraborty, N. Solca, O. Dopfer, Angew. Chem. Int. Ed. 49 (2010) 10145–10148.
[36] O. Dopfer and N. Solca, Angew. Chem. Int. Ed. 3628–3631 (2002).
[37] K. Müller-Dethlefs, O. Dopfer, T.G. Wright, Chem. Rev. 94 (1994) 1845–1871.
[38] F. Filsinger, D.-S. Ahn, G. Meijer, G. von Helden, Phys. Chem. Chem. Phys. 14 (2012) 13370–13377.
[39] J. Zhang, L. Chen, W.M. Freund, W. Kong, J. Chem. Phys. 143 (2015) 74201.
[40] L. Chen, J. Zhang, W.M. Freund, W. Kong, J. Chem. Phys. 143 (2015) 44310.
[41] F. Bierau, P. Kupser, G. Meijer, G. von Helden, Phys. Rev. Lett. 105 (2010).
[42] D. Gerlich, Adv. Chem. Phys. 1 (1992).
[43] O. Asvany, S. Brünken, L. Kluge, S. Schlemmer, Appl. Phys. B 114 (2013) 203–211.
[44] J.G. Redwine, Z.A. Davis, N.L. Burke, R.A. Oglesbee, S.A. McLuckey, T.S. Zwier, Int. J. Mass Spectrom. 348 (2013) 9–14.
[45] I. Alata, J. Bert, M. Broquier, C. Dedonder, G. Feraud, G. Grégoire, S. Soorkia, E. Marceca, C. Jouvet, J. Phys. Chem. A 117 (2013) 4420–4427.
[46] J. Jašík, J. Zabka, J. Roithová, D. Gerlich, Int. J. Mass Spectrom. 354–355 (2013) 204–210.
[47] O.V. Boyarkin, V. Kopysov, Rev. Sci. Instrum. 85 (2014) 33105.
[48] S. Lee, D. Hauser, O. Lakhmanskaya, S. Spieler, E.S. Endres, K. Geistlinger, S.S. Kumar, R. Wester, Phys. Rev. A 93 (2016) 32513.
[49] A. Svendsen, U.J. Lorenz, O.V. Boyarkin, T.R. Rizzo, Rev. Sci. Instrum. 81 (2010) 73107.
[50] H. Hock, J.B. Kim, M.L. Weichman, T.I. Yacovitch, D.M. Neumark, J. Chem. Phys. 137 (2012) 244201.
[51] A. Luca, S. Schlemmer, I. Cermak, D. Gerlich, Rev. Sci. Instrum. 72 (2001) 2900–2908.
[52] D.J. Goebbert, T. Wende, R. Bergmann, G. Meijer, K.R. Asmis, J. Phys. Chem. A 113 (2009) 5874–5880.
[53] D. Neuwirth, J.F. Eckhard, K. Lange, B. Visser, M. Wiedemann, R. Schröter, M. Tschurl, U. Heiz, Int. J. Mass Spectrom. 387 (2015) 8–15.
[54] X.-B. Wang, L.-S.W. Rev, Sci. Instrum. 79 (2008) 73108.
[55] A. Masson, M.Z. Kamrath, M.A.S. Perez, M.S. Glover, U. Rothlisberger, D.E. Clemmer, T.R. Rizzo, J. Am. Soc. Mass Spectrom. 26 (2015) 1444–1454.
[56] U.J. Lorenz, T.R. Rizzo, Anal. Chem. 83 (2011) 7895–7901.
[57] S. Dillinger, J. Mohrbach, J. Hewer, M. Gaffga, G. Niedner-Schatteburg, Phys. Chem. Chem. Phys. 17 (2015) 10358–10362.
[58] K. Hirsch, J.T. Lau, P. Klar, A. Langenberg, J. Probst, J. Rittmann, M. Vogel, V. Zamudio-Bayer, T. Möller, B. von Issendorff, J. Phys. B: At. Mol. Opt. Phys. 42 (2009) 154029.
[59] A. Langenberg, K. Hirsch, A. Ławicki, V. Zamudio-Bayer, M. Niemeyer, P. Chmiela, B. Langbehn, A. Terasaki, B. von Issendorff, J.T. Lau, Phys. Rev. B 90 (2014).
[60] V. Zamudio-Bayer, K. Hirsch, A. Langenberg, A. Lawicki, A. Terasaki, B. von Issendorff, J.T. Lau, J. Chem. Phys 143 (2015) 244318.
[61] D.Z. Keifer, T. Motwani, C.M. Teschke, M.F. Jarrold, J. Am. Soc. Mass Spectrom. 27 (2016) 1028–1036.
[62] See <https://www.tu-chemnitz.de/physik/ION/Technology/Piezo_Valve>.
[63] M.J. Frisch, G.W. Trucks, H.B. Schlegel, G.E. Scuseria, M.A. Robb, J.R. Cheeseman, G. Scalmani, V. Barone, B. Mennucci, G.A. Petersson, H. Nakatsuji, M. Caricato, X. Li, H.P. Hratchian, A.F. Izmaylov, J. Bloino, G. Zheng, J.L. Sonnenberg, M. Hada, M. Ehara, K. Toyota, R. Fukuda, J. Hasegawa, M. Ishida, T. Nakajima, Y. Honda, O. Kitao, H. Nakai, T. Vreven, J.A. Montgomery Jr., J.E. Peralta, F. Ogliaro, M. Bearpark, J.J. Heyd, E. Brothers, K.N. Kudin, V.N. Staroverov, R. Kobayashi, J. Normand, K. Raghavachari, A. Rendell, J.C. Burant, S.S. Iyengar, J. Tomasi, M. Cossi, N. Rega, N.J. Millam, M. Klene, J.E. Knox, J.B. Cross, V. Bakken, C. Adamo, J. Jaramillo, R. Gomperts, R.E. Stratmann, O. Yazyev, A.J. Austin, R. Cammi, C. Pomelli, J.W. Ochterski, R.L. Martin, K. Morokuma, V.G. Zakrzewski, G.A. Voth, P. Salvador, J.J. Dannenberg, S. Dapprich, A.D. Daniels, Ö. Farkas, J.B. Foresman, J.V. Ortiz, J. Cioslowski, D.J. Fox. Gaussian 09 D.01, Gaussian Inc., Wallingford CT, 2009.
[64] C.M. Choi, D.H. Choi, N.J. Kim, J. Heo, Int. J. Mass Spectrom. 314 (2012) 18–21.
[65] J.A. Stearns, S. Mercier, C. Seaiby, M. Guidi, O.V. Boyarkin, T.R. Rizzo, J. Am. Chem. Soc. 129 (2007) 11814–11820.
[66] S. Soorkia, M. Broquier, G. Gregoire, J. Phys. Chem. Lett. 5 (2014) 4349–4355.
[67] TURBOMOLE V6.2 2010 (1989–2007, a development of University of Karlsruhe and Forschungszentrum Karlsruhe GmbH), TURBOMOLE GmbH, since 2007 available from <http://www.turbomole.com>.
[68] C.M. Western, J. Quant. Spectrosc. Radiat. Transfer. (2016) http://dx.doi.org/10.1016/j.jqsrt.2016.04.010. in press.
[69] I. Pugliesi, K. Müller-Dethlefs, J. Phys. Chem. A 4657 (2006).
[70] A. Losi, Photochem. Photobiol. 83 (2007) 1283–1300.
[71] A. Losi, W. Gärtner, Photochem. Photobiol. 87 (2011) 491–510.
[72] T.E. Swartz, T.-S. Tseng, M.A. Frederickson, G. Paris, D.J. Comerci, G. Rajashekara, J.-G. Kim, M.B. Mudgett, G.A. Splitter, R.A. Ugalde, F.A. Goldbaum, W.R. Briggs, R.A. Bogomolni, Science 317 (2007) 1090–1093.
[73] Gunther L. Eichhorn (Ed.), Inorganic Biochemistry, vol. 2, The Structure and Reactivity of Flavin-Metal Complexes, 1973.

[74] E. Silva, A.M. Edwards, Flavins. Photochemistry and Photobiology, RSC Pub, Cambridge, UK, 2006.
[75] P. Nieto, A. Günther, G. Berden, J. Oomens, O. Dopfer, submitted for publication.
[76] J. Langer, A. Günther, S. Seidenbecher, G. Berden, J. Oomens, O. Dopfer, Chem. Phys. Chem. 15 (2014) 2550–2562.